Inorganic Chemistry
including bioinorganic chemistry

November 3, 2014
Volume 53, Number 21
pubs.acs.org/IC

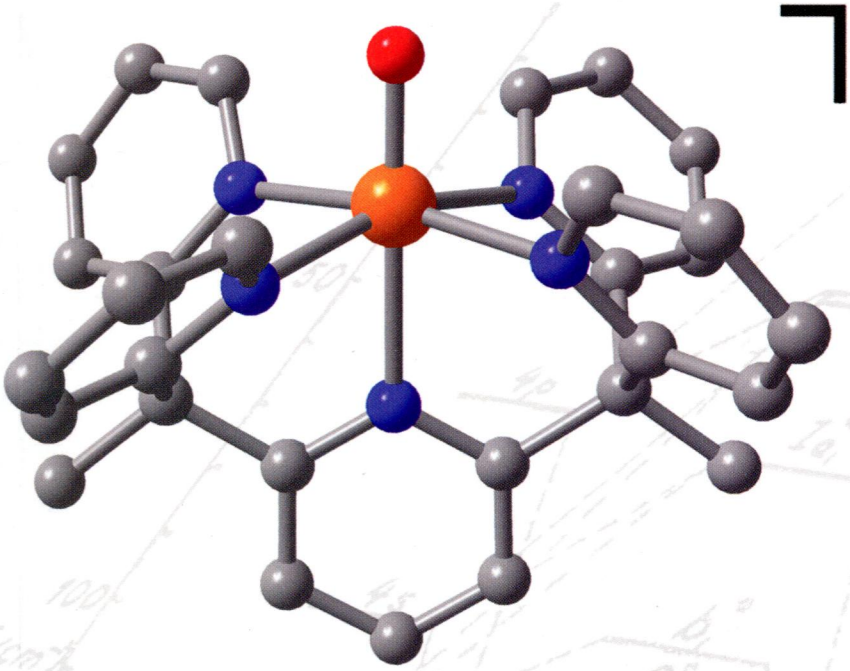

$[V^{III}O]^+$

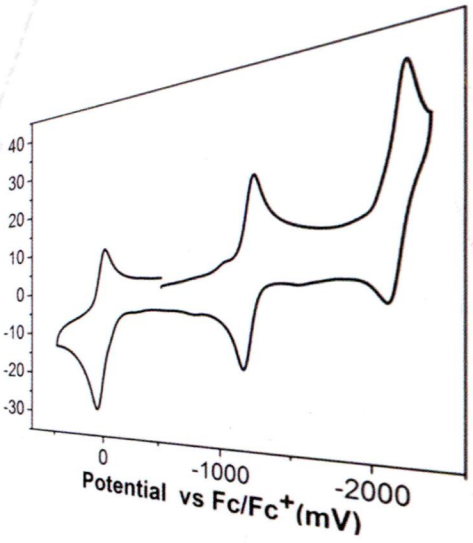

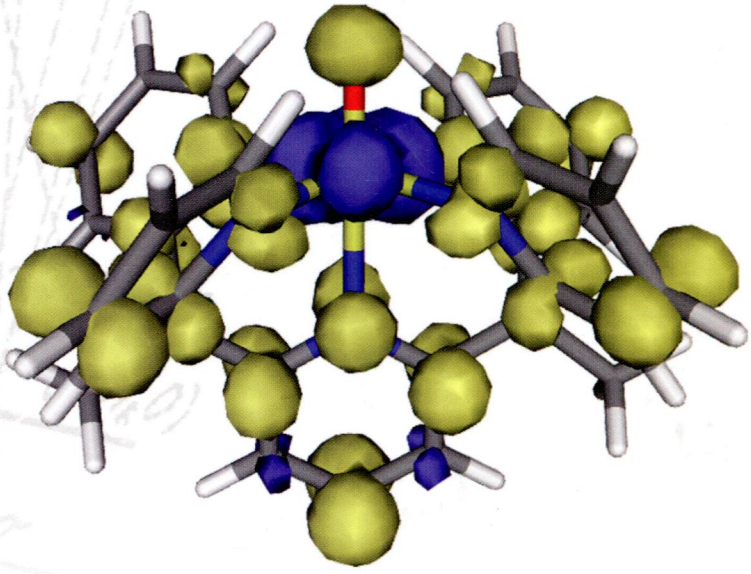

Low-Valent Vanadium Oxo Chemistry

ACS Publications
Most Trusted. Most Cited. Most Read.

www.acs.org

Inorganic Chemistry

NOVEMBER 3, 2014
VOLUME 53 ISSUE 21

INOCAJ 53(21) 11345−11808 (2014)
ISSN 0020-1669
Registered in the U.S. Patent and Trademark Office

ON THE COVER: The synthesis and characterization of a unique terminal mononuclear vanadium(III) oxo species supported by a pentadentate polypyridyl ligand are reported. Computational results predict that this $[V^{III}O]^+$ species features the lowest possible oxidation state of vanadium in this ligand environment. The results have important implications for future efforts toward low-valent vanadyl chemistry, particularly with regard to the isolation and study of formal vanadium(II) oxo species. [The cover background is a digitally modified version of Figure 3 from the article "The Electronic Structure of the Vanadyl Ion" by C. J. Ballhausen and Harry B. Gray (*Inorg. Chem.* **1962**, *1*, 111−122).] See A. E. King, M. Nippe, M. Atanasov, T. Chantarojsiri, C. A. Wray, E. Bill, F. Neese, J. R. Long, and C. J. Chang, p 11388.

Communications

11351 DOI: 10.1021/ic5022005

New Method for Exploring Deactivation Kinetics in Copper-Catalyzed Atom-Transfer-Radical Reactions
Timothy J. Zerk and Paul V. Bernhardt*

Copper(I) complexes may react with an alkyl halide to release an alkyl radical (activation). The kinetics of the reverse reaction between the alkyl radical and copper(II) complex are less studied because it is difficult to isolate or quantify the concentration of the alkyl radical ($R^{\bullet}$) in situ. We report a broadly applicable electrochemical technique for simultaneously measuring the kinetics of deactivation and kinetics of activation in these systems.

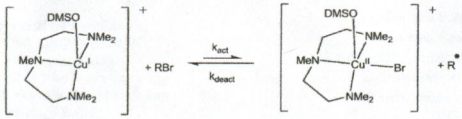

11354 DOI: 10.1021/ic5024218

Heterometallic Multiple Bonding: Delocalized Three-Center σ and π Bonding in Chains of 4d and 5d Transition Metals
David W. Brogden and John F. Berry*

$Mo_2Ru(dpa)_4Cl_2$ (**1**) and $W_2Ru(dpa)_4Cl_2$ (**2**) have short Mo–Ru and W–Ru distances, 2.38 Å (**1**) and 2.39 Å (**2**), indicating delocalized Mo–Mo–Ru and W–W–Ru bonding. Density functional theory calculations reveal the presence of both a three-center/two-electron σ bond and two three-center/four-electron π bonds in the compounds.

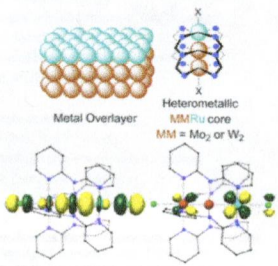

Articles

11357 DOI: 10.1021/ic501694d

Multinuclear Copper(I) and Silver(I) Amidinate Complexes: Synthesis, Luminescence, and CS_2 Insertion Reactivity
Andrew C. Lane, Matthew V. Vollmer, Charles H. Laber, Doris Y. Melgarejo, Gina M. Chiarella, John P. Fackler Jr., Xinzheng Yang, Gary A. Baker, and Justin R. Walensky*

Novel dinuclear Cu(I) and Ag(I) formamidinate complexes have been synthesized, and their reactivity has been probed with carbon disulfide insertion producing tetranuclear or hexanuclear clusters. Only the 2,6-dimethylphenyl derivative of the dinuclear Cu(I) formamidinate complex is luminescent, unlike the Ag(I) and Au(I) analogs, and shows reversible quenching with O_2.

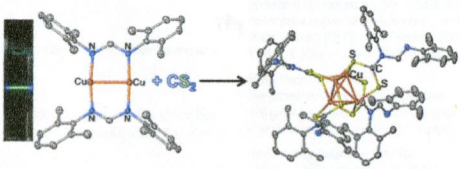

11367 S DOI: 10.1021/ic500926c

Small Bifunctional Chelators That Do Not Disaggregate Amyloid β Fibrils Exhibit Reduced Cellular Toxicity

Anuj K. Sharma, Jaekwang Kim, John T. Prior, Nicholas J. Hawco, Nigam P. Rath, Jungsu Kim, and Liviu M. Mirica*

Two small bifunctional chelators, L1 and L2, were developed to specifically target the interactions of Cu^{2+} and Zn^{2+} ions with the $A\beta_{42}$ peptide and to control the formation of neurotoxic $A\beta_{42}$ aggregates. Unprecedentedly, these compounds promote the fibrillization of Cu^{2+}-stabilized soluble $A\beta_{42}$ oligomers, and most importantly they drastically reduce the neurotoxicity of soluble $A\beta_{42}$ species, in both the presence or absence Cu^{2+} ions

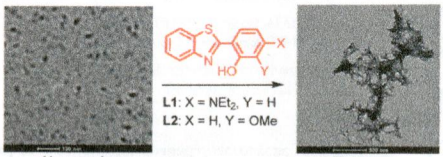

11377 S DOI: 10.1021/ic5018888

Oxidation of Alcohols and Activated Alkanes with Lewis Acid-Activated TEMPO

Thuy-Ai D. Nguyen, Ashley M. Wright, Joshua S. Page, Guang Wu, and Trevor W. Hayton*

$MCl_3(\eta^1$-TEMPO) (M = Fe, Al, TEMPO = 2,2,6,6-tetramethylpiperidine-*N*-oxyl) can oxidize a variety of alcohols and activated alkanes, including 1-phenyl-2-phenoxyethanol. However, in some instances overoxidation of substrate is observed, concomitant with incorporation of TEMPO into the products of oxidation.

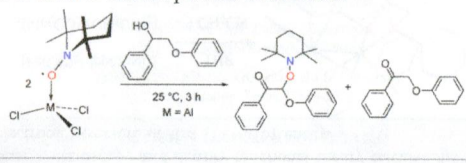

11388 S DOI: 10.1021/ic5010177

A Well-Defined Terminal Vanadium(III) Oxo Complex

Amanda E. King, Michael Nippe, Mihail Atanasov,* Teera Chantarojsiri, Curtis A. Wray, Eckhard Bill, Frank Neese,* Jeffrey R. Long,* and Christopher J. Chang*

The synthesis, characterization, and computational analysis of a unique terminal mononuclear vanadium(III) oxo species is presented. This low-valent vanadyl, supported by the pentadentate polypyridyl ligand 2,6-bis[1,1-bis(2-pyridyl)ethyl]pyridine ($PY5Me_2$), is reactive toward protons but not toward H- and O-atom-transfer reagents. Computations predict that further one-electron reduction of the vanadium(III) oxo species will result in ligand-based reduction, which has implications for the synthesis and reactivity of low-valent vanadyl species.

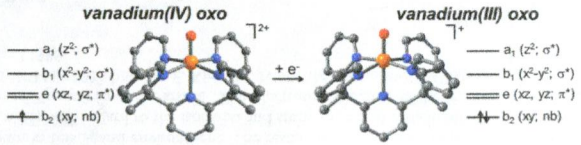

11396 DOI: 10.1021/ic501057r

Luminescence Properties and Energy Transfer of Eu/Mn-Coactivated $Mg_2Al_4Si_5O_{18}$ as a Potential Phosphor for White-Light LEDs

Jian Chen, Yangai Liu,* Minghao Fang, and Zhaohui Huang

A series of color-tunable blue–white emitting $Mg_2Al_4Si_5O_{18}$: Eu^{2+}, Mn^{2+} phosphors were prepared by a high-temperature solid-state reaction, and their luminescence properties were investigated. The energy-transfer mechanism was verified by the change in the luminescence spectra, decay curve, and energy-transfer efficiency of the phosphors, and the emission hue can be tuned from blue (0.17, 0.17) to bluish-green (0.22, 0.29) and finally to white (0.31, 0.33) emissions by properly varying the ratio of Eu^{2+}/Mn^{2+}.

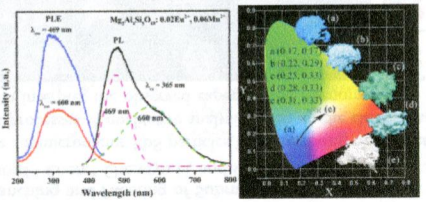

11404 DOI: 10.1021/ic501778d

Interaction of Chromium(III) with a *N,N′*-Disubstituted Hydroxylamine-(diamido) Ligand: A Combined Experimental and Theoretical Study

Petros A. Tziouris, Constantinos G. Tsiafoulis, Manolis Vlasiou, Haralampos N. Miras,* Michael P. Sigalas,* Anastasios D. Keramidas,* and Themistoklis A. Kabanos*

Interaction of *trans*-$[Cr^{III}Cl_2(H_2O)_4]Cl{\cdot}2H_2O$ with the *N,N′*-disubstituted hydroxylamine-(diamido) ligandHhydia gives $[Cr^{III}(Hhydia)_2]Cl_3$ (**1**) as a major species. The X-ray structure analysis of **1** revealed that the chromium atom in $[Cr^{III}(Hhydia)_2]^{3+}$ is bonded to two neutral tridentate *O,N,O*-Hhydia ligands. The two intramolecular hydrogen bonds in $[Cr(Hhydia)_2]^{3+}$ contribute to its stability.

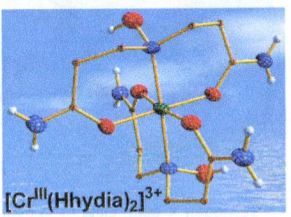

11415 DOI: 10.1021/ic501107a

Bonding and Charge Transfer in Nitrogen-Donor Uranyl Complexes: Insights from NEXAFS Spectra

C. D. Pemmaraju,* Roy Copping, Shuao Wang, Markus Janousch, Simon. J. Teat, Tolek Tyliszcak, Andrew Canning, David K. Shuh, and David Prendergast

The electronic structures of recently synthesized uranyl ($\{UO_2\}^{2+}$) complexes $[UO_2(H_2bbp)Cl_2]$, $[UO_2(Hbbp)(Py)Cl]$, and $[UO_2(bbp)(Py)_2]$, featuring the polarizable nitrogen-donor ligand 2,6-bis(2-benzimidazyl)pyridine (bbp), are investiagted through N K-edge NEXAFS spectroscopy measurements and first-principles simulations. Spectral features reveal both the polarization of the largely π-conjugated framework of the bbp ligand upon complexation with uranyl as well as trends in bbp–uranyl bonding across the three complexes, driven by chemical differences in the coordination shell of the uranyl moiety.

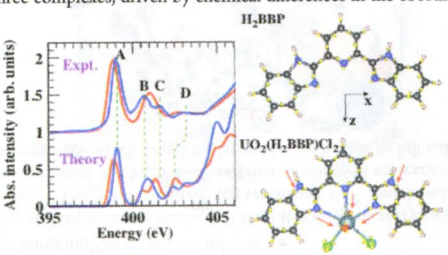

11426 S

DOI: 10.1021/ic501216d

Synthesis, Characterization, X-ray Crystal Structure, DFT Calculations, and Catalytic Properties of a Dioxidovanadium(V) Complex Derived from Oxamohydrazide and Pyridoxal: A Model Complex of Vanadate-Dependent Bromoperoxidase

Chandrima Das, Piyali Adak, Satyajit Mondal, Ryo Sekiya, Reiko Kuroda, Serge I. Gorelsky,* and Shyamal Kumar Chattopadhyay*

A vanadium(V) complex with the formula $[Et_3NH][V^VO_2(sox\text{-}pydx)]$ with new tridentate ligand soxH-pydxH, obtained by condensation of oxamohydrazide and pyridoxal, is found to possess exceptionally high catalytic efficiency (k_{cat} = 26340 h^{-1}) in peroxidative bromination of the model substrate phenol red to bromophenol blue. The vanadium compound also efficiently catalyzes bromination of phenol and salicylaldehyde as well as oxidation of benzene to phenol by H_2O_2.

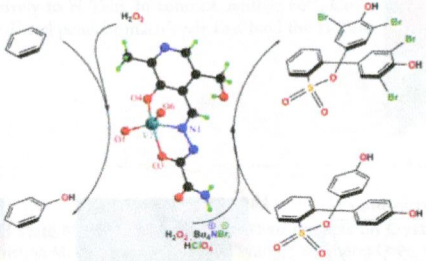

11438 S

DOI: 10.1021/ic5012082

Transition-Metal Complexes Containing Parent Phosphine or Phosphinyl Ligands and Their Use as Precursors for Phosphide Nanoparticles

Susanne Bauer, Cornelia Hunger, Michael Bodensteiner, Wilfried-Solo Ojo, Arnaud Cros-Gagneux, Bruno Chaudret, Céline Nayral, Fabien Delpech, and Manfred Scheer*

The P–H functional complexes $[(CO)_xM(\mu\text{-}PH_2)]_2$ (M = Fe, x = 3; M = Cr, W, x = 4) were synthesized in a one pot reaction by using $P_2(SiMe_3)_4$. Alternatively, photolysis of $[(CO)_3M(PH_3)_3]$ (M = Cr (**5a**), M = W (**5b**)) or of $[(CO)_xM(\mu\text{-}PH_2)]_2$ with $P(SiMe_3)_3$ leads to $[(CO)_4M(\mu\text{-}PH_2)_2M(CO)_3(PH_3)]$ (M = Cr (**3a**), M = W (**3b**)) and $[(CO)_4W(\mu\text{-}PH_2)_2W(CO)_2(PH_3)_2]$ (**4b**). Complex **2a** was used as single source precursor for the stoichiometry-controlled synthesis of CrP nanoparticles.

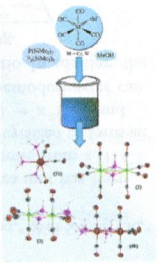

11447 S

DOI: 10.1021/ic501248c

Synthesis of Tridentate 2,6-Bis(imino)pyridyl Ruthenium(II) Complexes with N-Heterocyclic Carbene Ligands: Activation of Imidazolium Salts

Hyojong Yoo* and Donald H. Berry

Tridentate 2,6-bis(imino)pyridyl ruthenium(II) complexes with hydride and N-heterocyclic carbene ligands were successfully synthesized through the activation of imidazolium salts by low-valent Ru(0) complexes. A zwitterionic ruthenium complex with an ylidic ligand, bis(imino)pyridyl ruthenium-(2-methyleneimidazoline) complex, was also isolated. Formation mechanisms of these complexes are proposed and discussed.

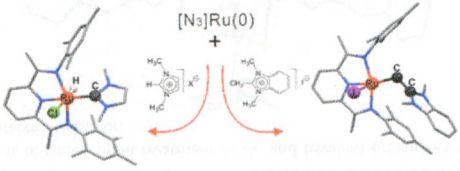

11457 DOI: 10.1021/ic501284y

Single-Component and Warm-White-Emitting Phosphor $NaGd(WO_4)_2$:Tm^{3+}, Dy^{3+}, Eu^{3+}: Synthesis, Luminescence, Energy Transfer, and Tunable Color

Yan Liu, Guixia Liu,* Jinxian Wang, Xiangting Dong, and Wensheng Yu

Tm^{3+}, Dy^{3+}, and Eu^{3+} single, double, and triple doped octahedral $NaGd(WO_4)_2$ microcrystals were prepared by hydrothermal process. The energy migration of Tm^{3+}–Dy^{3+}–Eu^{3+}, utilized for sensitizing Eu^{3+} ions besides compensating the red component at low Eu^{3+} doping concentration, has been discussed first. Under 365 nm excitation, the color-tunable emissions are realized, especially warm white emission, which could be favorable candidates in full-color phosphors for nUV-LEDs.

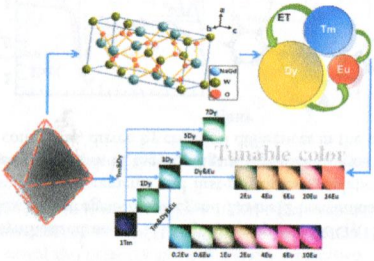

11467 DOI: 10.1021/ic501329p

Rational Design of Superoxide Dismutase (SOD) Mimics: The Evaluation of the Therapeutic Potential of New Cationic Mn Porphyrins with Linear and Cyclic Substituents

Artak Tovmasyan, Sebastian Carballal, Robert Ghazaryan, Lida Melikyan, Tin Weitner, Clarissa G. C. Maia, Julio S. Reboucas, Rafael Radi, Ivan Spasojevic, Ludmil Benov, and Ines Batinic-Haberle*

Mn porphyrins (MnPs) with linear and cyclic substituents were synthesized and evaluated for their *in vitro* and *in vivo* therapeutic potential. The $E_{1/2}$ of the $Mn^{III}P/Mn^{II}P$, which parallels $k_{cat}(O_2^{\bullet-})$ and $k_{red}(ONOO^-)$, controls the magnitude of lipid peroxidation inhibition by MnPs, and their ability to protect SOD-deficient yeast growth and to catalyze ascorbate oxidation.

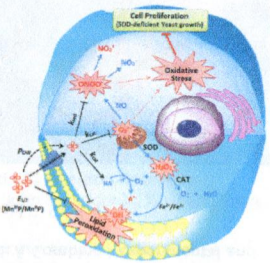

11484 DOI: 10.1021/ic501368y

Local Supersaturation Dictated Branching and Faceting of Submicrometer PbS Particles with Cubic Growth Habit

Mingzhu Liu, Mei Leng, Dan Liu, Fanglin Chen,* Chengyu Li, and Cheng Wang*

Three kinds of hierarchical cubelike submicrometer PbS particles that consisting of truncated octahedrons, cuboctahedrons, and cubes were obtained in solution processes. A qualitative analysis based on the classical nucleation theory coupled with the crystal growth theory is employed to interpret the observed experimental phenomena.

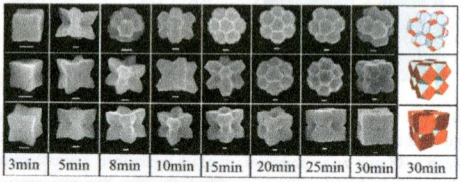

11492 Ⓢ DOI: 10.1021/ic501404v

Chromium–Chromium Interaction in a Binuclear Mixed-Valent Cr^{I}–Cr^{II} Complex

Ahmed Alzamly, Serge I. Gorelsky, Sandro Gambarotta,* Ilia Korobkov, Jennifer Le Roy, and Muralee Murugesu

A mixed-valent Cr^{I}–Cr^{II} species is obtained upon treatment of di- and trivalent precursors with Me_3Al. The presence of a Cr–Cr double bond prevents catalytic behavior.

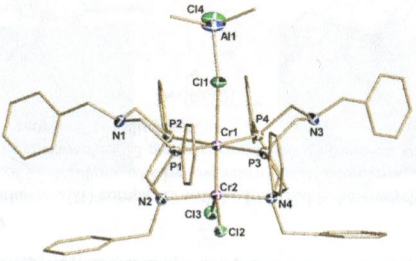

11498 Ⓢ DOI: 10.1021/ic501417s

Turn-on Phosphorescent Chemodosimeter for Hg^{2+} Based on a Cyclometalated Ir(III) Complex and Its Application in Time-Resolved Luminescence Assays and Live Cell Imaging

Jia-Xi Ru, Li-Ping Guan, Xiao-Liang Tang,* Wei Dou, Xiang Yao, Wan-Min Chen, Ya-Ming Liu, Guo-Lin Zhang,* Wei-Sheng Liu,* Yue Meng, and Chun-Ming Wang

A novel phosphorescent chemodosimeter based on a cyclometalated Ir(III) complex containing a thiourea unit has been successfully synthesized and characterized. The complex exhibits weak phosphorescence, which mainly comes from a ^{3}ILCT excited state according to TD-DFT calculations. In the presence of Hg^{2+}, the thiourea unit of the ligand is cyclized to form an imidazoline moiety, resulting in stronger phosphorescence attributed to an admixture of ^{3}MLCT ($d\pi(Ir) \rightarrow \pi^*(L)$) and ^{3}LLCT ($\pi(ppy) \rightarrow \pi^*(L)$). Furthermore, by using a time-resolved photoluminescence technique, the chemodosimeter can eliminate the interference from the short-lived background fluorescence and improve the signal-to-noise ratio. In addition, the chemodosimeter can be used to monitor Hg^{2+} effectively in living cells by confocal luminescence imaging.

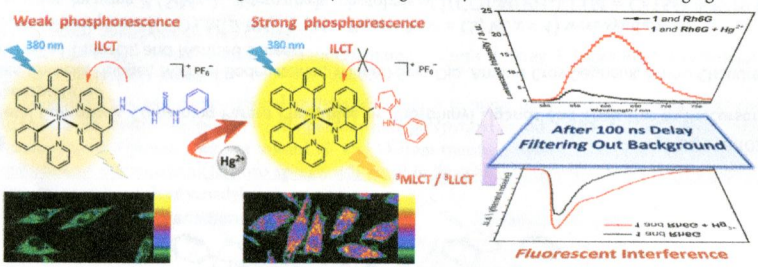

11507 Ⓢ

DOI: 10.1021/ic5014347

Speciation of Ferric Phenoxide Intermediates during the Reduction of Iron(III)–μ-Oxo Dimers by Hydroquinone

William D. Kerber,* Kaitlyn A. Perez, Chuqiao Ren, and Maxime A. Siegler

Iron(III) is chelated by tris(pyridylmethyl)amine to form $[Fe(TPA)]^{+3}(aq)$ at low pH and the μ-oxo dimer $[Fe_2(\mu\text{-}O)(TPA)_2(H_2O)_2]^{+4}$ above pH 3. The dimer is a diprotic acid with $pK_{a1,2}$ = 4.38 and 5.26. Addition of a phenol displaces solvent from the labile coordination sites to form ferric phenoxide complexes that have a pH-dependent speciation. When the incoming phenol is hydroquinone, the complex is reduced to iron(II) with concomitant formation of benzoquinone.

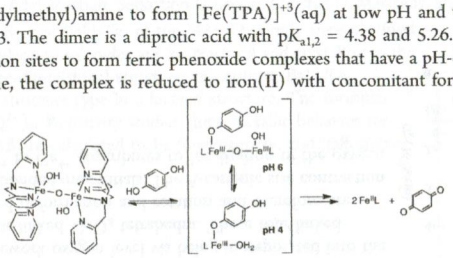

11517 Ⓢ

DOI: 10.1021/ic501463q

X-ray Absorption and Emission Spectroscopies of X-Bridged Diiron Phthalocyanine Complexes $(FePc)_2X$ (X = C, N, O) Combined with DFT Study of $(FePc)_2X$ and Their High-Valent Diiron Oxo Complexes

Cedric Colomban, Evgenij V. Kudrik, Valerie Briois, Janine C. Shwarbrick, Alexander B. Sorokin,* and Pavel Afanasiev*

A series of μ-bridged diiron phthalocyanine complexes [PcFeXFePc] (X = C, N, O) was studied by core hole spectroscopies at the Fe K edge, including EXAFS, XES, and resonant XANES. Spectroscopy-calibrated DFT calculations provide a coherent description of the molecular geometry and electronic structure. Theory calculations extrapolated to the high-valent putative oxo complexes of three diiron species allow explaining of the outstanding catalytic activity of the μ-nitrido complex as compared to its μ-oxo and μ-carbido counterparts.

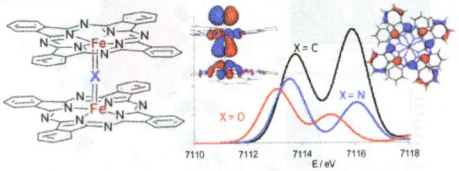

11531 Ⓢ

DOI: 10.1021/ic501411w

Relationships between Electron Density and Magnetic Properties in Water-Bridged Dimetal Complexes

Jacob Overgaard,* James P. S. Walsh, Venkatesha R. Hathwar, Mads R. V. Jørgensen, Christina Hoffman, Jamie A. Platts, Ross Piltz, and Richard E. P. Winpenny

The experimental and theoretical electron density distributions in two structurally similar transition metal dimers (M = Ni, Co; see Figure) were analyzed using the atoms-in-molecules (AIM) approach, and selected properties related to the chemical bonding are compared to measured intramolecular magnetic exchange interaction parameters.

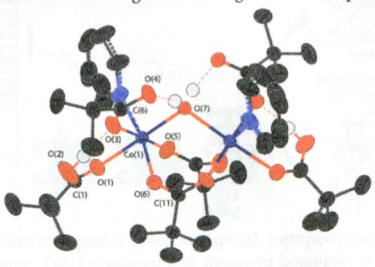

11540 Ⓢ

DOI: 10.1021/ic501484p

Selective Binding of Zn^{2+} Complexes to Human Telomeric G-Quadruplex DNA

Kevin E. Siters, Matthew A. Fountain,* and Janet R. Morrow*

Two Zn^{2+} macrocyclic complexes are studied as binders for thymine-containing sequences in the loops of the human telomeric (H-Telo) G-quadruplex. Data support the selective binding of a Zn^{2+} complex with a dansyl pendent to thymine nucleobases in the lateral loops of H-Telo. The Zn^{2+} complex containing an acridine pendent binds tightly but nonselectively to H-Telo. In contrast, neither Fe^{2+}, Co^{2+}, nor Cu^{2+} forms complexes with the dansyl pendent macrocycle that bind the H-Telo G-quadruplex.

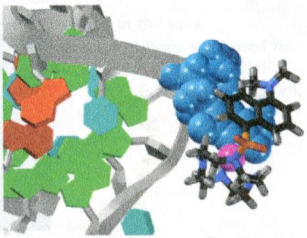

11552 Ⓢ

DOI: 10.1021/ic5015835

Intermolecular Interactions in Solid-State Metalloporphyrins and Their Impacts on Crystal and Molecular Structures

Seth C. Hunter, Brenda A. Smith, Christina M. Hoffmann,* Xiaoping Wang,* Yu-Sheng Chen, Garry J. McIntyre, and Zi-Ling Xue*

Hirshfeld surface analyses reveal *intermolecular* interactions in the crystals of [M(TPP)X] (TPP^{2-} = *meso*-tetraphenylporphyrinate; M = Fe, X = Cl; M = Co, Fe, X = NO) lead to phase changes in [M(TPP)(NO)] and a gradual structural change in [Fe(TPP)Cl], allowing reversible thermal compression at lower temperatures.

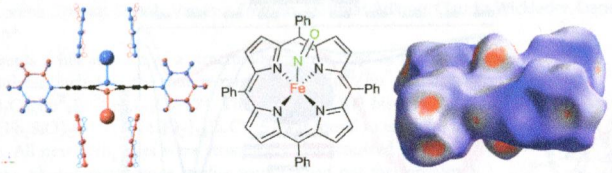

11563 Ⓢ

DOI: 10.1021/ic501624b

Large Thermal Hysteresis for Iron(II) Spin Crossover Complexes with *N*-(Pyrid-4-yl)isonicotinamide

Charles Lochenie, Wolfgang Bauer, Antoine P. Railliet, Stephan Schlamp, Yann Garcia,* and Birgit Weber*

Iron(II) spin crossover materials with wide hysteresis loops are obtained due to a combination of short-range (hydrogen bonds) and long-range (coordination polymer) interactions.

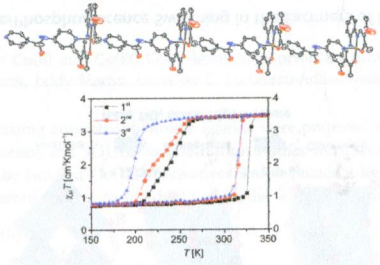

11573 S DOI: 10.1021/ic501613a

Making Oxidation Potentials Predictable: Coordination of Additives Applied to the Electronic Fine Tuning of an Iron(II) Complex

Stefan Haslinger, Jens W. Kück, Eva M. Hahn, Mirza Cokoja, Alexander Pöthig, Jean-Marie Basset, and Fritz E. Kühn*

This work examines the impact of axially coordinating additives on the electronic structure of an iron(II) complex, inspired by apical coordination in biological systems. The predictability of oxidation potentials is demonstrated, based on a correlation between cyclic voltammetry experiments and density functional theory calculated molecular orbital energies.

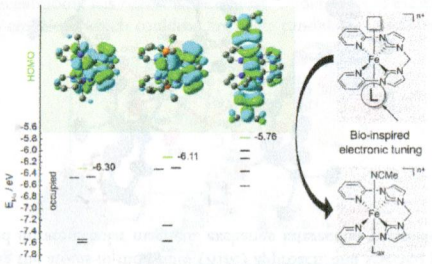

11584 S DOI: 10.1021/ic501657p

A Nanosized {Ag@Ag_{12}} "Molecular Windmill" Templated by Polyoxometalates Anions

Lei Wang, Weiting Yang, Wei Zhu, Xingang Guan, Zhigang Xie,* and Zhong-Ming Sun*

A nanosized molecular windmill-shaped polynuclear Ag cluster with intriguing {$M@M_{12}$}-type cuboctahedral topology with effective photocatalytic and antibacterial activities templated by POMs.

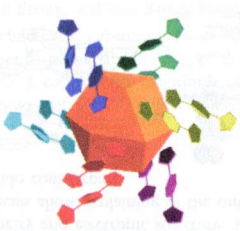

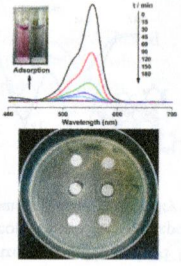

11589 S DOI: 10.1021/ic501662p

Localization of Oxygen Interstitials in $CeSrGa_3O_{7+\delta}$ Melilite

Jungu Xu, Xiaojun Kuang,* Emmanuel Véron, Mathieu Allix, Matthew R. Suchomel, Florence Porcher, Chaolun Liang, Fengjuan Pan, and Mingmei Wu*

The excess oxygen atoms from the oxidation of Ce^{3+} to Ce^{4+} in $CeSrGa_3O_{7+\delta}$ melilite are localized at the framework oxygen level via being incorporated into the coordination environment of four-linked GaO_4 tetrahedra. These four-linked tetrahedral units have constrained deformation and rotation and therefore are unfavorable for transporting the bonded interstitials. The A-cationic size contraction induced by the oxidation of Ce^{3+} to Ce^{4+} contributes to localization of the oxygen interstitials.

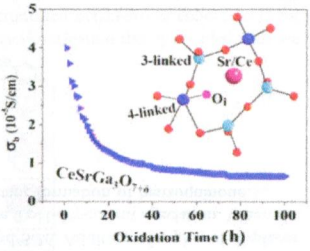

11598 DOI: 10.1021/ic501571u

Compressibility and Structural Stability of Nanocrystalline TiO_2 Anatase Synthesized from Freeze-Dried Precursors

Catalin Popescu,* Juan Angel Sans, Daniel Errandonea, Alfredo Segura, Regina Villanueva, and Fernando Sapiña

The HP structural behavior of anatase-type nanoparticles was studied using X-ray diffraction under hydrostatic and quasi-hydrostatic conditions up to 25 GPa. Experiments were carried out by the first time under hydrostatic conditions. An anatase-baddeleyite phase transition is found under compression. On decompression a columbite-type structure is recovered as a metastable phase. Possible mechanisms for the observed phase transition are discussed. Results are compared with previous HP studies on anatase nanoparticles.

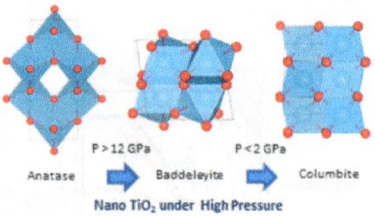

11604 DOI: 10.1021/ic5016687

Mechanically Triggered Fluorescence/Phosphorescence Switching in the Excimers of Planar Trinuclear Copper(I) Pyrazolate Complexes

Qiong Xiao, Ji Zheng, Mian Li, Shun-Ze Zhan, Jun-Hao Wang, and Dan Li*

A series of cyclic trinuclear copper(I) pyrazolate clusters with auxochrome-appended ligands have been found to exhibit unusual luminescence mechanochromism, featuring switchable fluorescent and phosphorescent bands in dual emission.

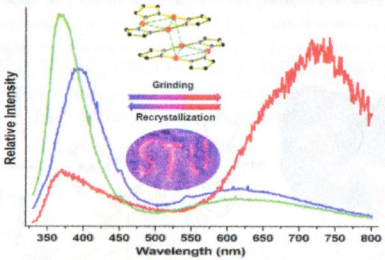

11616 DOI: 10.1021/ic501770g

Synthesis, Crystal Structure, and Electronic Properties of High-Pressure PdF_2-Type Oxides MO_2 (M = Ru, Rh, Os, Ir, Pt)

Yuichi Shirako,* Xia Wang, Yoshihiro Tsujimoto, Kie Tanaka, Yanfeng Guo, Yoshitaka Matsushita, Yoshihiro Nemoto, Yoshio Katsuya, Youguo Shi, Daisuke Mori, Hiroshi Kojitani, Kazunari Yamaura, Yoshiyuki Inaguma, and Masaki Akaogi

The polycrystalline MO_2's (HP-PdF_2-type MO_2, M = Rh, Os, Pt) with high-pressure PdF_2 compounds were successfully synthesized under high-pressure and high-temperature conditions for the first time, to the best of our knowledge.

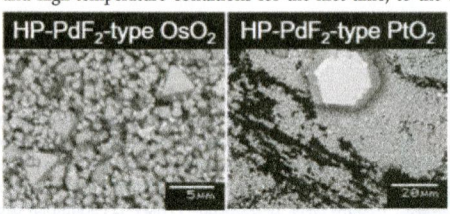

11626 S

DOI: 10.1021/ic501795w

Syntheses, Crystal Structures, Transport Properties, and Theoretical Studies of Five Members of the MAn_2Q_5 Family: SrU_2S_5, BaU_2Se_5, PbU_2S_5, $BaTh_2S_5$, and BaU_2Te_5

Jai Prakash, Mariya S. Tarasenko, Adel Mesbah, Sébastien Lebègue, Christos D. Malliakas, and James A. Ibers*

SrU_2S_5, BaU_2Se_5, PbU_2S_5, $BaTh_2S_5$, and BaU_2Te_5 of the MAn_2Q_5 family were obtained by solid-state reactions. The sulfides and selenides are isostructural and crystallize in the PbU_2Se_5 structure type in a three-dimensional structure; in contrast, BaU_2Te_5 crystallizes in the $(NH_4)Pb_2Br_5$ structure type in a layered structure. The formulas charge balance as $M^{2+}(An^{4+})_2(Q^{2-})_5$. Resistivity studies show metallic behavior for SrU_2S_5, BaU_2Se_5, and PbU_2S_5. All are calculated to be ferromagnetic and half-metals.

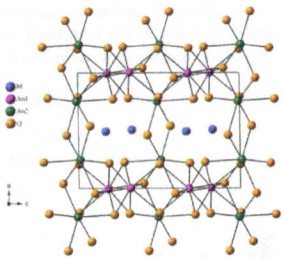

11633 S

DOI: 10.1021/ic501766k

The Curious Case of Mesityl Azide and Its Reactivity with $bpyNiEt_2$

Brooke M. Otten, Travis M. Figg, and Thomas R. Cundari*

DFT analysis of the reaction of $bpyNiEt_2$ with ArN_3 is performed for *ortho*- and *para*-tolyl, *meta*-xylyl, and mesityl azide ($MesN_3$). Of interest are the different products obtained for the latter (ethylene, butane, azomesitylene, *N*-mesityl-ethylamine) versus the other reagents: (bpyNi(N(Ar)Et)(Et)). Metal-free reactions do not differentiate $MesN_3$ from other azides. Calculated Ni–N/C bond energies suggest the role of radicals in discriminating among these reactions, and that their concentration will be greatest for $MesN_3$.

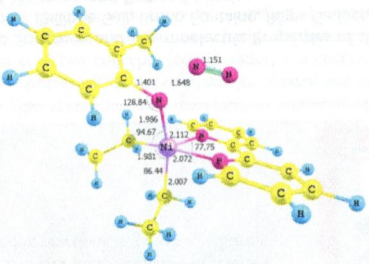

11640 S

DOI: 10.1021/ic501831j

Xenon(IV)–Carbon Bond of $[C_6F_5XeF_2]^+$; Structural Characterization and Bonding of $[C_6F_5XeF_2][BF_4]$, $[C_6F_5XeF_2][BF_4]\cdot 2HF$, and $[C_6F_5XeF_2][BF_4]\cdot n NCCH_3$ (n = 1, 2); and the Fluorinating Properties of $[C_6F_5XeF_2][BF_4]$

Karsten Koppe, Jamie Haner, Hélène P. A. Mercier, Hermann-J. Frohn,* and Gary J. Schrobilgen*

The X-ray crystal structures of the first Xe(IV)–C bonded species, $[C_6F_5XeF_2]^+$, were determined in the salts $[C_6F_5XeF_2][BF_4]$, $[C_6F_5XeF_2][BF_4]\cdot 2HF$, and $[C_6F_5XeF_2][BF_4]\cdot 1.5NCCH_3$. Quantum-chemical calculations were used to arrive at detailed vibrational (Raman) assignments, as well as the NBO analyses and MO descriptions of the $[C_6F_5XeF_2]^+$ cation and the isoelectronic $C_6F_5IF_2$ molecule. The ^{19}F and ^{129}Xe NMR spectra of $[C_6F_5XeF_2]^+$ and $C_6F_5IF_2$ were simulated, and their spin–spin couplings were fully assigned.

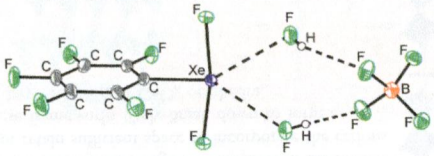

$[C_6F_5XeF_2][BF_4]\cdot 2HF$

11662 S

DOI: 10.1021/ic501837x

Heterometallic Europium Disiloxanediolates: Synthesis, Structural Diversity, and Photoluminescence Properties

Janek Rausch, Volker Lorenz, Cristian G. Hrib, Vanessa Frettlöh, Matthias Adlung, Claudia Wickleder, Liane Hilfert, Peter G. Jones, and Frank T. Edelmann*

This contribution presents a full account of a structurally diverse class of heterometallic europium disiloxanediolates, including the unique mixed-valent Eu^{III}/Eu^{II} disiloxanediolate cluster $[(Ph_2SiO)_2O]_6Eu^{II}_4Eu^{III}_2Li_4O_2Cl_2$ (**7**). The europium(III) bis(disiloxanediolate) $[\{(Ph_2SiO)_2O\}_2\{Li(THF)_2\}_2]EuCl$ (**5**) was found to exhibit a brilliant red triboluminescence. All new complexes were structurally characterized by X-ray diffraction. Furthermore, photoluminescence studies were carried out for complex **5** showing an excellent color quality, due to the strong $^5D_0 \rightarrow {}^7F_2$ transition, but a weak antenna effect.

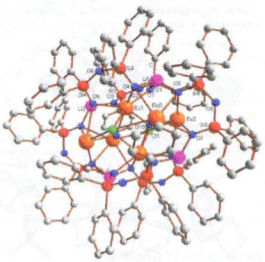

11675 S

DOI: 10.1021/ic501883z

Synthesis and Structural Features of Co(II) and Co(III) Complexes Supported by Aminotrisphenolate Ligand Scaffolds

Carmen Martín, Christopher J. Whiteoak, Eddy Martin, Eduardo C. Escudero-Adán, José Ramón Galán-Mascarós, and Arjan W. Kleij*

Co(II) and Co(III) complexes comprising aminotrisphenolate ligands were prepared and fully characterized. X-ray analyses, variable-temperature NMR measurements, and SQUID magnetization studies were conducted to support the oxidation states of the obtained complexes. One of the isolated Co(III) derivatives shows fluxional ligand coordination behavior in solution allowing for penta- and hexa-coordinated species to be identified in the high- and low-temperature regimes, respectively.

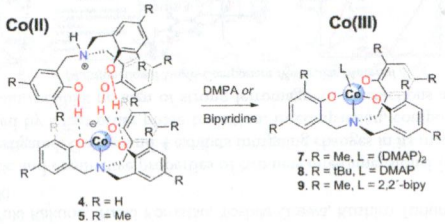

4. R = H
5. R = Me

7. R = Me, L = $(DMAP)_2$
8. R = tBu, L = DMAP
9. R = Me, L = 2,2′-bipy

11682 S DOI: 10.1021/ic501905v

A New Class of Azadipnictiridines Generated by an Unusual Rearrangement Reaction

Alexander Hinz, Axel Schulz,* Wolfram W. Seidel, and Alexander Villinger

Dipnictadiazanediyls add readily alkynes affording [2.1.1]bicycles, which rearrange slowly to [3.1.0]bicycles resulting in the formation of novel azadipnictiridines.

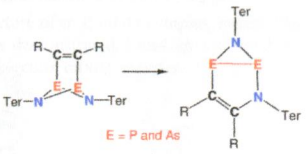

11691 S DOI: 10.1021/ic501726m

Synthesis and Crystal Structure of δ-TaON, a Metastable Polymorph of Tantalum Oxide Nitride

Tobias Lüdtke, Alexander Schmidt, Caren Göbel, Anna Fischer, Nils Becker, Christoph Reimann, Thomas Bredow, Richard Dronskowski, and Martin Lerch*

Tetragonal anatase-type δ-TaON was prepared by reaction of gaseous ammonia with an amorphous tantalum oxide precursor. At temperatures between 800 and 850 °C an irreversible phase transformation to baddeleyite-type β-TaON is observed. Quantum-chemical calculations confirm the dynamic stability of δ-TaON. It was found that an N/O distribution with maximal N–N distances is most stable. The calculated band edge energies indicate that δ-TaON is a promising photocatalytic material for redox reactions, e.g., water splitting.

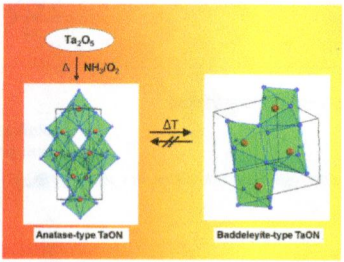

11699 S DOI: 10.1021/ic501939k

X-ray Characterization, Electronic Band Structure, and Thermoelectric Properties of the Cluster Compound $Ag_2Tl_2Mo_9Se_{11}$

Rabih Al Rahal Al Orabi, Patrick Gougeon,* Philippe Gall, Bruno Fontaine, Régis Gautier, Malika Colin, Christophe Candolfi, Anne Dauscher, Jiri Hejtmanek, Bernard Malaman, and Bertrand Lenoir

The novel Mo-based cluster compound $Ag_2Tl_2Mo_9Se_{11}$ shows glass-like thermal conductivity due to a strong disorder induced by the Ag and Tl atoms, leading to interesting thermoelectric properties at high temperatures.

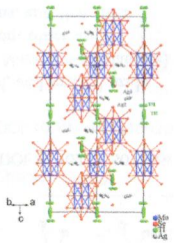

11710 S

DOI: 10.1021/ic5019532

Multifunctional One-Dimensional Rhodium(I)–Semiquinonato Complex: Substituent Effects on Crystal Structures and Solid-State Properties

Minoru Mitsumi,* Shoji Ohtake, Yuki Kakuno, Yuuki Komatsu, Yoshiki Ozawa, Koshiro Toriumi, Nobuhiro Yasuda, Nobuaki Azuma, and Yuji Miyazaki

The crystal structures and magnetic and conductive properties of two new one-dimensional (1D) rhodium(I)–semiquinonato complexes **4** and **5** have been investigated. Compound **4** exhibits intriguing changes in its magnetic and conducting properties, and these changes are accompanied by a first-order phase transition. In comparison, compound **5**, which assumes a strongly dimerized structure in the 1D chain, exhibits no sign of strong ferromagnetic interactions and is an insulator.

Multifunctional Single-Component Molecular Material

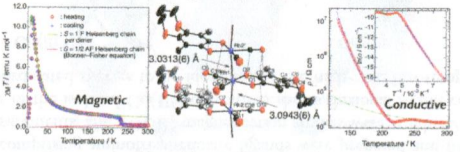

11721 S

DOI: 10.1021/ic501963y

Novel Barium–Organic Incorporated Iodometalates: Do They Have Template Properties for Constructing Rare Heterotrimetallic Hybrids?

Shashank Mishra,* Erwann Jeanneau, Gilles Ledoux, and Stéphane Daniele*

Novel barium-organic incorporated iodocuprates and -argentates retain their structural motifs when a MI_4 tetrahedral/MI_3 trigonal-coplanar unit is replaced by another $M'I_4$/$M'I_3$ unit. Such structure-directing properties are, however, not observed when a MI_4/MI_3 unit is replaced by a $M'I_6$ octahedron, which requires molecular rearrangement.

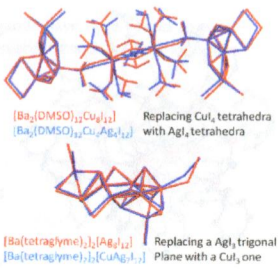

11732 S

DOI: 10.1021/ic501958y

Postperovskite Phase Transition of $ZnGeO_3$: Comparative Crystal Chemistry of Postperovskite Phase Transition from Germanate Perovskites

Hitoshi Yusa,* Taku Tsuchiya, Masaki Akaogi, Hiroshi Kojitani, Daisuke Yamazaki, Naohisa Hirao, Yasuo Ohishi, and Takumi Kikegawa

The rotation of the GeO_6 octahedra in perovskites is thought to be closely related to the postperovskite transition. In the perovskites with large divalent cations, the corner-sharing GeO_6 frameworks could not retain sufficient space to incorporate the cations by increasing the tilting angle. These frameworks likely break down to form a postperovskite structure without a large rotation of GeO_6 octahedra.

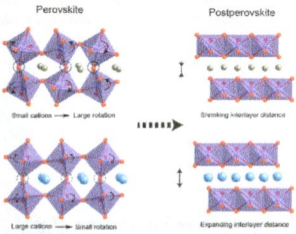

11740 DOI: 10.1021/ic502015c

Multimetallic Complexes and Functionalized Nanoparticles Based on Unsymmetrical Dithiocarbamate Ligands with Allyl and Propargyl Functionality

Venesia L. Hurtubise, James M. McArdle, Saira Naeem, Anita Toscani, Andrew J. P. White, Nicholas J. Long,* and James D. E. T. Wilton-Ely*

Unsymmetrical dithiocarbamate ligands prove to be versatile starting points for the preparation of both multimetallic complexes and surface-functionalized gold nanoparticles. The ligands provide a platform for functional group transformations of the pendant alkene or alkyne functionality, while cyclization of the propargyl derivative provides an atom-efficient and high-yielding route to thiazolidine-2-thiones.

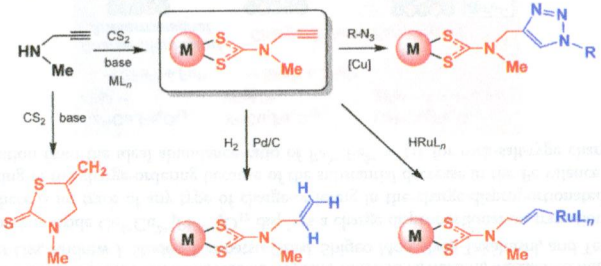

11749 DOI: 10.1021/ic5020175

Cocrystallization of Photosensitive Energetic Copper(II) Perchlorate Complexes with the Nitrogen-rich Ligand 1,2-Di(1*H*-tetrazol-5-yl)ethane

Jürgen Evers, Ivan Gospodinov, Manuel Joas, Thomas M. Klapötke,* and Jörg Stierstorfer

The preparation and characterization of an energetic ionic cocrystal consisting of copper(II) as a central metal ion, 1,2-di(1*H*-tetrazol-5-yl)ethane as a ligand, and perchlorate as a counterion is, beside further coordination compounds, presented. This ionic cocrystal represents the combination of two concepts (complexation and cocrystallization) in designing energetic materials. Further, different coordination spheres within the cocrystal (octahedral and square pyramidal) were shown by UV/vis/NIR spectroscopy to result in high light absorption and, therefore, an increased sensitivity toward laser irradiation.

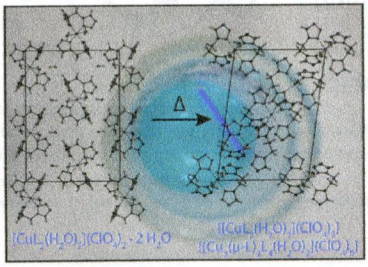

11757 S

DOI: 10.1021/ic502044d

An Acentric Calcium Borate $Ca_2[B_5O_9]\cdot(OH)\cdot H_2O$: Synthesis, Structure, and Nonliner Optical Property

Qi Wei, Jian-Wen Cheng,* Chao He, and Guo-Yu Yang*

A new acentric hilgardite-type calcium borate, $Ca_2[B_5O_9]\cdot(OH)\cdot H_2O$ (**1**), was made under solvothermal condition. Its framework features a denser net with interpenetrated *pcu* B–O net and *dia* Ca–O net. **1** is a potential deep-UV NLO material with a strong SHG response ~3 times that of KH_2PO_4 (KDP) and a short UV cutoff edge below 200 nm.

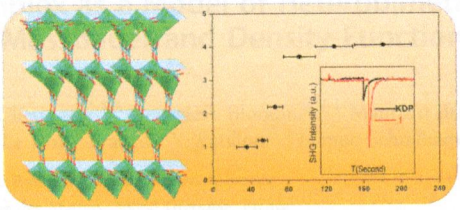

11764 S

DOI: 10.1021/ic502071u

Continuous Control of Optical Gaps in Quasi-One-Dimensional Bromide-Bridged Platinum Complexes by Utilizing Chemical Pressure

Shohei Kumagai, Hiroaki Iguchi, Shinya Takaishi,* Brian K. Breedlove, Masahiro Yamashita,* Hiroyuki Matsuzaki, Hiroshi Okamoto, Kenichi Kato, and Masaki Takata

Bromide-bridged Pt chain complexes, $[Pt(en)_2Br](C_n{-}Y)_2\cdot H_2O$ (en = ethylenediamine; C_n–Y = dialkyl sulfosuccinate; n = the number of carbon atoms), were synthesized. The Pt–Pt distances and the optical gaps depended on n and T. In addition, $[Pt(en)_2Br](C_{12}{-}Y)_2\cdot H_2O$ had the shortest Pt–Pt distance among the bromide-bridged Pt chain complexes reported so far.

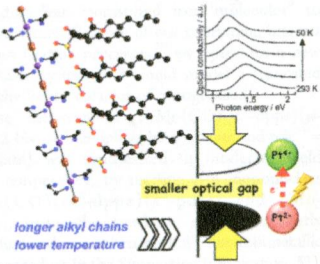

11770 S

DOI: 10.1021/ic5020785

Dinuclear Nickel Complexes in Five States of Oxidation Using a Redox-Active Ligand

You-Yun Zhou, Douglas R. Hartline, Talia J. Steiman, Phillip E. Fanwick, and Christopher Uyeda*

Dinuclear Ni complexes were synthesized using a redox-active naphthyridine–diimine (NDI) ligand system. Cyclic voltammetry experiments reveal rich, reversible redox chemistry for this platform, enabling access to a series of five $(NDI)Ni_2$ complexes related by electron transfer. The members of this series were characterized using structural and spectroscopic methods in combination with DFT models. The interplay between metal- and ligand-centered redox activity is discussed.

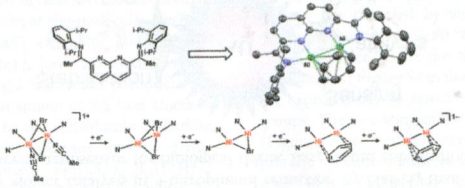

11778 (S) DOI: 10.1021/ic502080x

Tetrapalladium-Containing Polyoxotungstate $[Pd^{II}_4(\alpha\text{-}P_2W_{15}O_{56})_2]^{16-}$: A Comparative Study

Natalya V. Izarova, Raisa I. Maksimovskaya, Sabine Willbold, and Paul Kögerler*

Pd^{II}-based sandwich complexes of lacunary $\{P_2W_{15}\}$-type polyoxotungstates differ markedly from classical dimeric $\{M_4(P_2W_{15})_2\}$ structures incorporating octahedral first-row transition metal M^{II} centers, form syn and anti isomers in a characteristic 2:1 ratio, and exhibit high stability in solution.

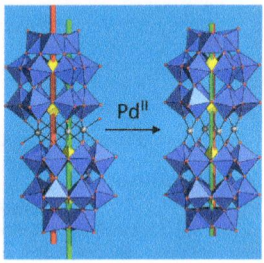

11785 DOI: 10.1021/ic502081c

A First-Principles Approach to the Calculation of the on-Site Zero-Field Splitting in Polynuclear Transition Metal Complexes

Marius Retegan, Nicholas Cox, Dimitrios A. Pantazis, and Frank Neese*

A new high-level multireference method is developed for the calculation of the on-site zero-field splitting parameters. The applicability of the method is demonstrated using a series of Mn(III)-containing complexes of increasing nuclearity, including the inorganic cluster of the water-splitting complex of photosystem II.

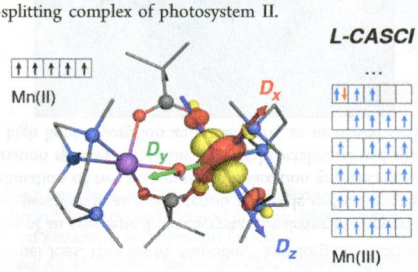

11794 (S) DOI: 10.1021/ic502138v

Charge-Order Melting in Charge-Disproportionated Perovskite $CeCu_3Fe_4O_{12}$

Ikuya Yamada,* Hidenobu Etani, Makoto Murakami, Naoaki Hayashi, Takateru Kawakami, Masaichiro Mizumaki, Shigenori Ueda, Hideki Abe, Klaus-Dieter Liss, Andrew J. Studer, Tomoatsu Ozaki, Shigeo Mori, Ryoji Takahashi, and Tetsuo Irifune

A novel quadruple perovskite oxide $Ce^{4+}Cu^{2+}{}_3Fe^{3.5+}{}_4O_{12}$ displays a charge disproportionation transition of $4Fe^{3.5+} \rightarrow 3Fe^{3+} + Fe^{5+}$ below ~270 K. There is no trace of any type of charge-ordering in the charge-disproportionated $CeCu_3Fe_4O_{12}$ phase, demonstrating the melting of the charge-ordering because of the substantial decrease in the Fe valence from tetravalency and the resulting large deviation from the ideal abundance ratio of Fe^{3+}:Fe^{5+} = 1:1 for rock-salt-type charge-ordering.

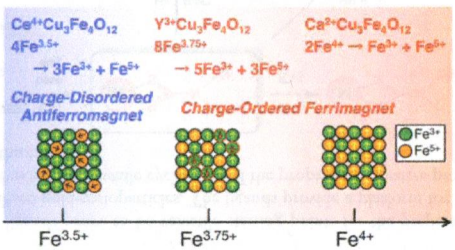

DOI: 10.1021/ic5021498

Stabilization of AuNPs by Monofunctional Triazole Linked to Ferrocene, Ferricenium, or Coumarin and Applications to Synthesis, Sensing, and Catalysis

Na Li, Pengxiang Zhao, María E. Igartua, Amalia Rapakousiou, Lionel Salmon, Sergio Moya, Jaime Ruiz, and Didier Astruc*

Ferrocene and coumarin triazole (Cou-trz) were utilized to stabilize gold nanoparticles (AuNPs). The first ferricenium-stabilized AuNP was directly obtained by the reaction between the trz-linked ferrocene and $HAuCl_4$. Ferrocene- and ferricenium-appended **AuNP-1** and **AuNP-2** reversibly interconvert. The trz-linked ferricenium chloride stabilization of **AuNP-2** is also characterized by slower catalysis in 4-nitrophenol reduction by $NaBH_4$ than with other trz-AuNPs. **AuNP-3** capped with Cou-trz is a fluorescent nanosensor for biological thiols. Easy ligand substitution was also applied to dendrimer synthesis.

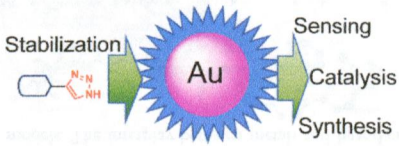

Ⓢ Supporting Information available via online article